International Journal of Geographical Information Science, 2014
http://dx.doi.org/10.1080/13658816.2014.924628

Taylor & Francis
Taylor & Francis Group

A new pseudocylindrical equal-area projection for adaptive composite map projections

Bojan Šavrič* and Bernhard Jenny

College of Earth, Ocean, and Atmospheric Sciences, Oregon State University, Corvallis, OR, USA

(*Received 25 February 2014; final version received 9 May 2014*)

The recently introduced adaptive composite map projection technique changes the projection to the geographic area shown on a map. It is meant as a replacement for the commonly used web Mercator projection, which grossly distorts areas when representing the entire world. The original equal-area version of the adaptive composite map projection technique uses the Lambert azimuthal projection for regional maps and three alternative projections for world maps. Adaptive composite map projections can include a variety of other equal-area projections when the transformation between the Lambert azimuthal and the world projections uses Wagner's method. To select the most suitable pseudocylindrical projection, the distortion characteristics of a pseudocylindrical projection family are analyzed, and a user study among experts in the area of map projections is carried out. Based on the results of the distortion analysis and the user study, a new pseudocylindrical projection is recommended for extending adaptive composite map projections. The new projection is equal-area throughout the transformation to the Lambert azimuthal projection and has better distortion characteristics then small-scale projections currently included in the adaptive composite map projection technique.

Keywords: pseudocylindrical projection; adaptive composite map projections; Wagner's transformation; web mapping; web Mercator projection

1. Introduction: projections for web maps

Web map authors have two options when selecting a map projection for an interactive web map. They can apply the same projection for all scales – which inevitably results in excessively distorted maps at some scales – or they can adjust the projection when the user changes map scale or the extent of the mapped area. When Google introduced its mapping service in 2005, with the Mercator projection used for all map scales, it made the Mercator projection the de-facto standard for web maps. Today, the Mercator projection is commonly used for web maps by all major web mapping services. While the conformal Mercator projection has advantages for maps at large scales, it is not well suited for small-scale mapping because it shows the areas close to poles with enormous areal distortion. This characteristic makes the Mercator projection an inappropriate choice for small-scale maps, especially when the area of features or the density of features is being compared. The Mercator projection also produces a map with infinite scale at the poles, which are therefore impossible to display. Consequently, the web Mercator projection only displays areas up to approximately 85° north and south (Figure 1).

*Corresponding author. Email: savricb@geo.oregonstate.edu

Figure 1. The web Mercator projection.

Adaptive composite map projections have recently been presented as an alternative to the static web Mercator projection (Jenny 2012). This composite of map projections smoothly transforms between different well-known map projections. Various projections are combined according to the extent of the area shown on the map and the central latitude of the mapped area, resulting in digital maps that can be equal-area for any map extent (Jenny 2012).

The adaptive composite map projection technique combines projections according to John P. Snyder's selection guideline for map projections (Snyder 1987). The Lambert azimuthal projection is the key element of the adaptive composite map projection technique. In accordance with Snyder's recommendation, the Lambert azimuthal projection is used with oblique aspects for regional maps that show areas the size of a hemisphere or a continent.

At larger scales, a combination of the Lambert cylindrical, the polar Lambert azimuthal, and the Albers conic projections are used (for details see Snyder 1987; Jenny 2012). The non-equal area Mercator projection is included for compatibility with existing web mapping services only at very large scales, allowing for a seamless transition to the Mercator raster tiles used by current web mapping services.

A variety of alternative projections for world maps can be combined with adaptive composite map projections by blending between small- and medium-scale projections (Jenny and Patterson 2013, Jenny and Šavrič in Press). However, projection blending does not result in equal-area projections. The equal-area world map projections for the adaptive composite map projection technique are currently limited to the Hammer, the Eckert–Greifendorff, and the quartic authalic projections. These three small-scale world projections can be converted into the medium-scale Lambert azimuthal projection, retaining the equal-area property throughout the transformation. David Aitoff introduced this transformation in 1889 (Aitoff 1889, Snyder 1993). It multiplies the abscissa of the Lambert azimuthal projection by a selected factor (marked as B on Figure 2) and divides longitudes by the same factor value (Equation 1) (Bugayevskiy and Snyder 1995). The value of factor B changes with the map extent in the adaptive composite map projections equations (Jenny 2012). Figure 2 presents a sequence of map projections where the value of B grows from 1 to infinity.

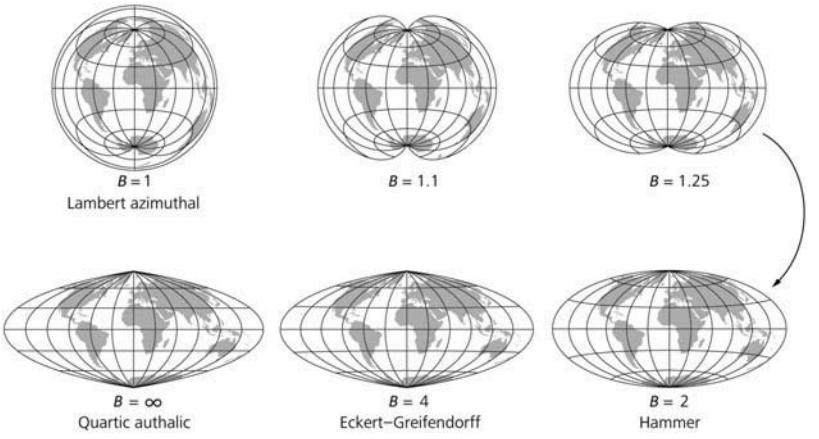

Figure 2. Transforming the Lambert azimuthal projection to the Hammer, the Eckert–Greifendorff, or the quartic authalic projection using Aitoff's transformation method. The B factor of Equation (1) straightens the parallels to create a pseudocylindrical projection for $B = \infty$.

$$x = \frac{B\sqrt{2}\cos\phi\sin(\lambda/B)}{\sqrt{1+\cos\phi\cos(\lambda/B)}}$$
$$y = \frac{\sqrt{2}\sin\phi}{\sqrt{1+\cos\phi\cos(\lambda/B)}} \quad (1)$$

where x and y are the projected coordinates, ϕ and λ are the latitude and longitude, and B is the transformation factor.

For uninterrupted equal-area world maps, aside from the Hammer projection, Snyder (1987) recommends pseudocylindrical projections, that is, projections with straight parallels and curved meridians. The easy comparison of areas at the same latitude is one advantage of pseudocylindrical projections. However, forcing the parallels of equal-area projections to remain straight will unavoidably introduce distortion in peripheral parts of the map. In non-pseudocylindrical projections, a slight bending of the parallels can reduce this distortion.

The only pseudocylindrical projection so far included with adaptive composite map projections is the quartic authalic projection. It represents the poles as points, which considerably distorts polar areas. Most equal-area pseudocylindrical projections representing poles as lines have better distortion properties than projections representing poles as points. Unfortunately, Aitoff's transformation method always results in projections representing the poles as points and not as lines (Figure 2).

The goal of the research presented in this article is to develop a small-scale pseudocylindrical projection with a pole line for adaptive composite map projections. This offers users an alternative to the quartic authalic projection, for cases when they do not wish to use a projection with curved parallels, such as the Hammer or Wagner VII projections.

An appropriate small-scale pseudocylindrical projection has to meet the following criteria. It should represent the poles as lines to minimize the distortion of areas at high latitudes. It should be equal-area to allow for the comparison of areas. It should be transformable to the Lambert azimuthal projection, and it should retain the equal-area

property throughout this transformation. Despite the large number of small-scale projections invented in the past, one cannot find a projection meeting all of these requirements (e.g., in projection directories and code libraries, such as Canters and Decleir 1989, Snyder and Voxland 1989, Snyder 1993, or Evenden 2008). We use a method introduced by Karl Heinrich Wagner (see the following section) for transforming the Lambert azimuthal projection to various world map projections. This transformation results in a variety of pseudocylindrical as well as non-pseudocylindrical projections. In this article, we are analyzing the pseudocylindrical family and proposing a new pseudocylindrical projection for adaptive composite map projections.

In the following sections, first, Wagner's transformation method is presented as an alternative to Aitoff's method for transforming the Lambert azimuthal projection to world map projections. After giving an overview of possible projections that can be created using Wagner's method, methods for analyzing the pseudocylindrical projection family are presented, including a user study, where map projection experts design a pseudocylindrical projection. The final section compares four candidate pseudocylindrical projections obtained from the analyses and proposes one of the four for inclusion in the adaptive composite map projection technique.

2. Wagner's transformation method

In 1932, the German cartographer Karl Heinrich Wagner suggested a transformation technique for the development of new map projections, which he referred to as *Umbeziffern*, meaning renumbering (Wagner 1931, 1932, 1941, 1949, 1962, 1982, Canters 2002). Tobler (1964) translated the term to 're-labeling.' Wagner (1932, 1949, 1962) presented three variations of this technique, with one maintaining the area distortion characteristics of the parent projection. With this method, different equal-area projections with straight or curved parallels can be created. For example, Wagner (1941) derived the equal-area Wagner VII projection from the Lambert azimuthal equal-area projection using this method (Figure 3). For the purposes of this article, the term *Wagner's transformation* refers to this area-preserving method, which Canters (2002) calls Wagner's second transformation method.

Wagner's transformation method first maps the longitude and latitude values onto a segment of the globe (Steps 1 and 2 on Figure 3). The segment of the globe (Step 1 on Figure 3) is defined with a bounding parallel ϕ_B (mirrored along the equator), and a bounding meridian λ_B (mirrored along the central meridian). The entire mapped area is then projected onto this segment using an existing projection (Step 2 on Figure 3). After the projection, the graticule is enlarged to the parent projection's scale with a factor $1/\sqrt{m \cdot n}$ (Step 3 on Figure 3). The parameters m and n are computed with $m = \sin\phi_B$ and $n = \lambda_B/\pi$. The stretching factor k finally adjusts the graticule to the preferred equator/central meridian ratio (Wagner 1941). The result is a new map projection (Step 4 on Figure 3). Equation (2) below shows the general formula of Wagner's transformation method.

$$\begin{aligned} x &= \frac{k}{\sqrt{m \cdot n}} \cdot f_x(\theta, n\lambda) \\ y &= \frac{1}{k\sqrt{m \cdot n}} \cdot f_y(\theta, n\lambda) \end{aligned} \tag{2}$$

where $\sin\theta = m \cdot \sin\phi,\ m = \sin\phi_B,\ n = \lambda_B/\pi,\ k$ is the stretching factor, and f_x and f_y are the original map projection equations.

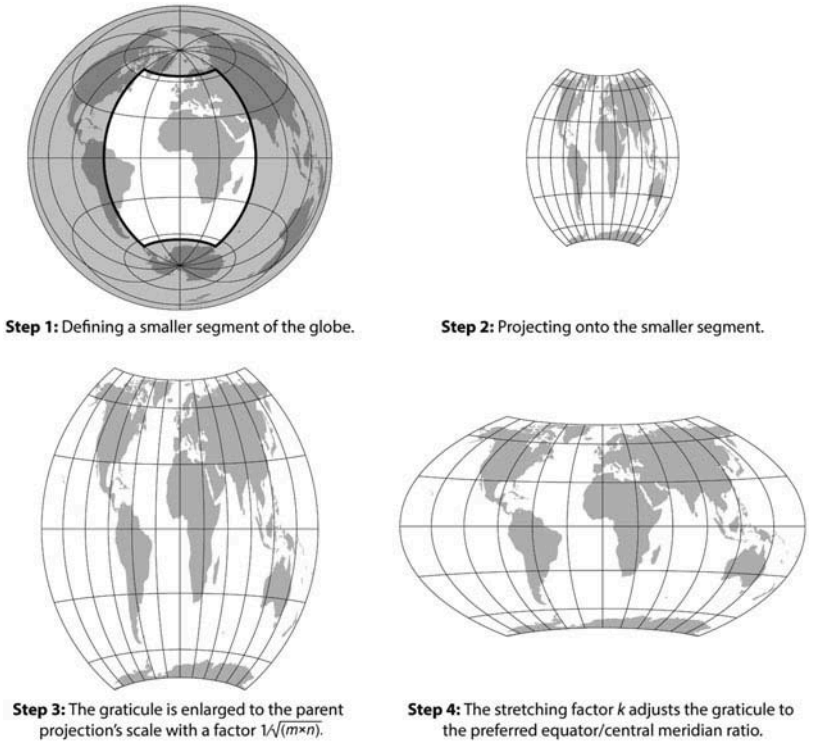

Figure 3. Wagner's steps in deriving the Wagner VII projection from the Lambert azimuthal equal-area projection using his transformation method (after Wagner 1941).

Karl Siemon (1936, 1937, 1938) formalized, expanded, and presented Wagner's ideas as a general theory of map projection transformation (Canters 2002). He also showed that Aitoff's transformation method is a special case of Wagner's area preserving transformation (Siemon 1937). Böhm (2006) presented projections created with Wagner's methods, some of which are compromise projections created with the method that Canters (2002) referred to as Wagner's third transformation method.

3. Map projections derived from the Lambert azimuthal projection

Applying Wagner's method to the Lambert azimuthal projection extends the set of small-scale map projections for the adaptive composite map projection technique. Equation (3) details the transformation of the Lambert azimuthal projection.

$$\begin{aligned} x &= \frac{k}{\sqrt{m \cdot n}} \cdot \frac{\sqrt{2} \cdot \cos\theta \, \sin n\lambda}{\sqrt{1 + \cos\theta \, \cos n\lambda}} \\ y &= \frac{1}{k\sqrt{m \cdot n}} \cdot \frac{\sqrt{2} \cdot \sin\theta}{\sqrt{1 + \cos\theta \, \cos n\lambda}} \end{aligned} \tag{3}$$

where x and y are the projected coordinates, ϕ and λ are the latitude and longitude, $\sin\theta = m \cdot \sin\phi$, n, m, and k are parameters for Wagner's transformation, defined as:

$m = \sin\phi_B$, $n = \lambda_B/\pi$, and $k = \sqrt{p \cdot \sin\frac{\phi_B}{2} / \sin\frac{\lambda_B}{2}}$, where ϕ_B and λ_B are the bounding parallel and the bounding meridian, and p is the equator/central meridian ratio.

Equation (4) is the inverse projection converting Cartesian coordinates to longitude and latitude.

$$\begin{aligned} \lambda &= \frac{1}{n} \cdot \arctan\left(\frac{Z \cdot X}{2 \cdot Z^2 - 1}\right) \\ \phi &= \arcsin\left(\frac{Z \cdot Y}{m}\right) \end{aligned} \tag{4}$$

where $X = x \cdot \sqrt{m \cdot n}/k$, $Y = y \cdot k \cdot \sqrt{m \cdot n}$, $Z = \sqrt{1 - (X^2 + Y^2)/4}$, and ϕ and λ are the latitude and longitude, x and y are the projected Cartesian coordinates, and n, m, and k are parameters for Wagner's transformation (see Equation 3).

Projections created from the Lambert azimuthal equal-area projection with Equation (3) are defined with three variables: (1) the bounding parallel ϕ_B, (2) the bounding meridian λ_B, and (3) the equator/central meridian ratio p. Since Wagner's transformation method preserves the equal-area property of the parent projection, the resulting projection will always be an equal-area projection. Figure 4 represents different projections created from the Lambert azimuthal projection. The bounding parallel ϕ_B is varied from 90° (top row) to 0° (bottom row). The bounding meridian λ_B is varied from 0° (left column) to 180° (right column). An equator/central meridian ratio $p = 2$ is applied to all graticules in Figure 4.

As shown by the graticules in Figure 4, the bending of parallels varies with the bounding meridian λ_B. Similarly, adjusting the bounding parallel ϕ_B changes the bending of the meridians. When the value of the bounding parameter decreases, parallels or meridians appear less bent. Setting both bounding values to 0° results in a cylindrical graticule with straight parallels and meridians (bottom left graticule in Figure 4). The bounding parallel also defines the length of the pole line. A bounding parallel of 0° sets the horizontal extent of the pole line to the length of the equator (bottom row in Figure 4). When the bounding meridian equals 180° and the bounding parallel equals 0°, the border meridians and pole lines have an infinite length.

A bounding parallel of 90° (top row in Figure 4) shows the poles as points. These projections represent Aitoff's transformation method that transforms between the Lambert azimuthal (top-right), the Hammer, the Eckert–Greifendorff, and the quartic authalic (top-left). All of the projections are stretched to an equator/central meridian ratio of $p = 2$. The intermediate graticule with a bounding meridian equal to 90° is the Hammer projection.

A bounding meridian at 0° longitude results in pseudocylindrical graticules (leftmost column in Figure 4). They are the limiting case when parameter n in Equation (3) approaches 0. Equation (5) is the forward projection and Equation (6) is the inverse projection for the pseudocylindrical projection family.

$$\begin{aligned} x &= \frac{k'}{\sqrt{m}} \cdot \frac{\lambda \cdot \cos\theta}{\cos(\theta/2)} \\ y &= \frac{2}{k'\sqrt{m}} \cdot \sin(\theta/2) \end{aligned} \tag{5}$$

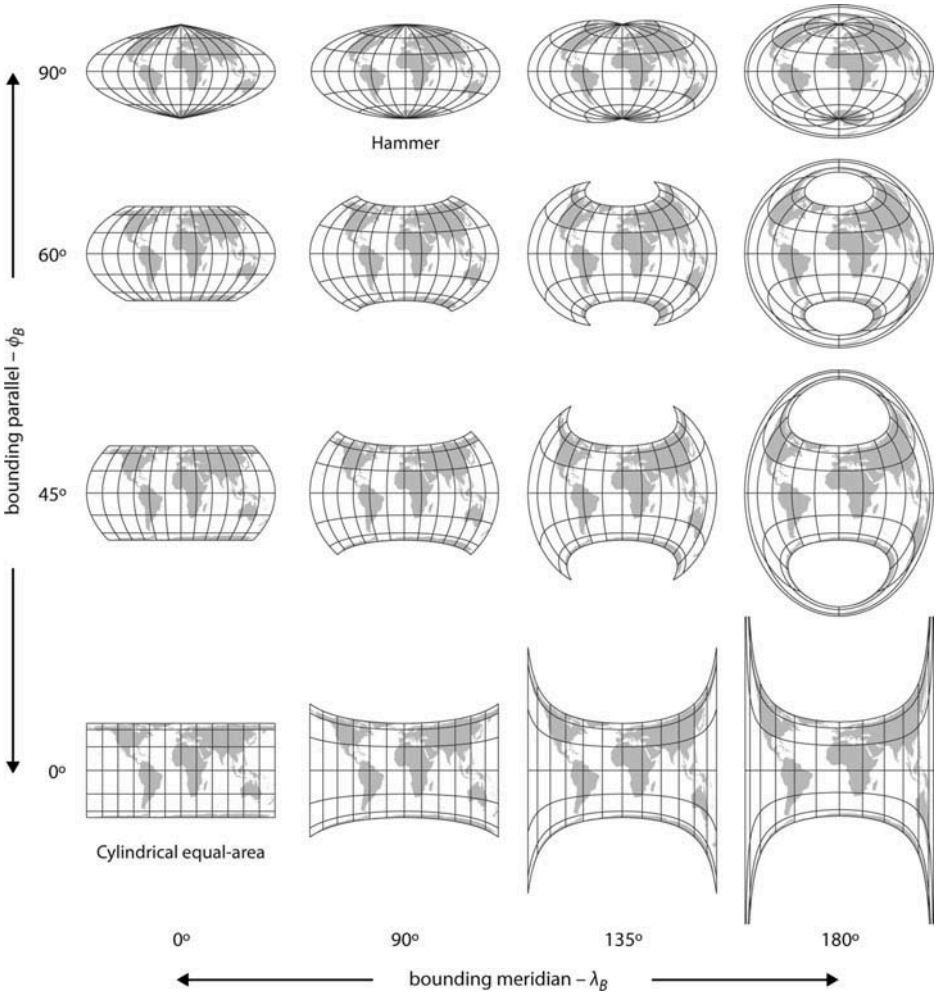

Figure 4. Different equal-area graticules derived from the Lambert azimuthal projection using Wagner's transformation method. The ratio between the lengths of the equator and the central meridian is 2:1 for all graticules.

$$\theta = 2 \cdot \arcsin\left(\frac{y \cdot k' \sqrt{m}}{2}\right)$$
$$\lambda = \frac{x\sqrt{m} \cdot \cos(\theta/2)}{k' \cdot \cos\theta} \tag{6}$$

where x and y are the projected coordinates, ϕ and λ are the latitude and longitude, $\sin\theta = m \cdot \sin\phi$, m and k' are parameters, defined as $m = \sin\phi_B$ and $k' = \sqrt{2 \cdot p \cdot \sin\frac{\phi_B}{2}/\pi}$, where ϕ_B is the bounding parallel and p is the equator/central meridian ratio.

The bending of the meridians and the length of the pole line both change with the bounding parallel for the pseudocylindrical projections. The pole line varies from a point

(when the bounding parallel is at 90°) to the length of the equator (when the bounding parallel is at 0°). The length of the pole line can also be described as the ratio between the equator and the pole line (q). For the pseudocylindrical projections derived with Equation (5), the ratio q can be computed directly from the bounding parallel ϕ_B and vice versa using Equation (7).

$$q = \frac{\cos(\phi_B/2)}{\cos\phi_B} \tag{7}$$

When the bounding parallel and bounding meridian are both equal to 0°, the result is the cylindrical equal-area projection family. The graticule of the cylindrical equal-area projection in Figure 4 (bottom left graticule) has a width-to-height ratio $p = 2$, which is the Smyth equal surface (Smyth 1870) or Craster's limiting case of hyperbolic equal-area projections (Craster 1929, Maling 1974) with a standard parallel at 37 °04′. The standard parallel ϕ_s of the cylindrical equal-area projection can be defined with the equator/central meridian ratio p. Using Equation (8), other cylindrical equal-area projections (e.g. the Lambert cylindrical equal-area) can be created from the Lambert azimuthal projection.

$$p = \pi \cdot \cos^2\phi_s \tag{8}$$

4. Methods for analyzing the equal-area pseudocylindrical projection family

With Wagner's transformation method, adaptive composite map projections can be extended with an entire family of small-scale map projections, as illustrated in Figure 4. While the graticules in the bottom right corner of Figure 4 are not useful, the pseudocylindrical projections in the leftmost column of Figure 4 are analyzed in this section. To select the most suitable pseudocylindrical projection, the projections are analyzed with two approaches. The first approach is a distortion analysis, where the overall angular and scale distortion indices are computed for a set of candidate projections, and projections with the best distortion properties are identified. The second approach takes the aesthetic appearance of the candidate projections into account. Map projection experts are asked to design a pseudocylindrical projection that appears the most graphically pleasing to them. In the following sections, both approaches are presented.

4.1. Distortion analysis

The distortion characteristics of map projections can be quantified with overall distortion measures. Since distortion varies throughout the mapped area, local metrics are aggregated by discretizing space and computing global distortion indices for the entire graticule. Canters and Decleir (1989) compare projections based on the mean scale, areal, and maximum angular distortion values. Goldberg and Gott (2007) add flexion and skewness indices. Čapek (2001) compares map projections using a distortion characterization indicator, the percentage ratio of area, where area and angular distortions are acceptable. In the map projection literature, scale distortion, area distortion, and maximum angular distortion are the three most commonly used measures (e.g. Snyder 1987, 1993, Canters and Decleir 1989, Canters 2002).

Since the candidate map projections in this study are all equal-area, their mean area distortion is zero. However, the mean scale distortion and the mean maximum angular

distortion values vary among projections. The weighted mean error in the overall scale distortion index D_{ab} and the mean angular deformation index D_{an} are computed for each candidate projection with Equation (9) (Canters and Decleir 1989, Canters 2002).

$$D_{ab} = \frac{1}{S}\sum_{i=1}^{k}\left(\frac{a_i^q + b_i^r}{2} - 1\right)\cos\phi_i \Delta\phi\Delta\lambda$$
$$D_{an} = \frac{1}{S}\sum_{i=1}^{k} 2\arcsin\left(\frac{a_i - b_i}{a_i + b_i}\right)\cos\phi_i \Delta\phi\Delta\lambda \tag{9}$$

where D_{ab} is the weighted mean error in the overall scale distortion, D_{an} is the mean angular deformation, a_i and b_i are the scale factors along the principal direction at the sample point, $S = \sum_{i=1}^{k}\cos\phi_i\Delta\phi\Delta\lambda$ is the sum of the area weight factors, ϕ_i is the sample point latitude, $\Delta\phi$ and $\Delta\lambda$ are intervals in the latitude and longitude, k is the number of sample points, and q and r coefficients are defined as

$$q = \begin{cases} 1 & a_i \geq 1 \\ -1 & a_i < 1 \end{cases}, \quad r = \begin{cases} 1 & b_i \geq 1 \\ -1 & b_i < 1 \end{cases}.$$

For the distortion analysis of the pseudocylindrical projection family, a set of candidate projections is created using Equation (5). The candidate projections differ in their bounding parallel ϕ_B and their equator/central meridian ratio p. The bounding parallel ϕ_B defines the bending of the meridians and the length of the pole line. Values vary from 0° (resulting in pole lines that have the same length as the equator) to 90° (resulting in poles that are represented as points). For this study, we vary the values for the equator/central meridian ratio p between 1 (the equator and the central meridian have the same length) and 3 (the equator is three times longer than the central meridian). A candidate projection is created for every half-degree of the bounding parallel ϕ_B and for every 0.01 unit change of the ratio p. This results in 181 × 201 candidate projections. For each candidate, the mean angular deformation index D_{an} and the weighted mean error in the overall scale distortion index D_{ab} are computed using Equation (9) for latitude and longitude intervals of 2.5° (as used by Canters and Decleir 1989). Finally, the projections with the best distortion indices are identified.

4.2. *User study with map projection experts*

A mathematics-based distortion analysis is a valuable tool for selecting a map projection. However, personal taste and aesthetic preference are also major selection criteria. To take this subjective aspect into account, experts in the area of map projections were invited to design a projection. The projections suggested by the experts were compiled and aggregated. The goal was to achieve a wider acceptance of the final projection for the adaptive composite map projection technique.

Forty-four experts were invited to select their favorite member of the pseudocylindrical equal-area family derived from the Lambert azimuthal projection using Wagner's transformation method. The invited experts have authored articles or web pages about

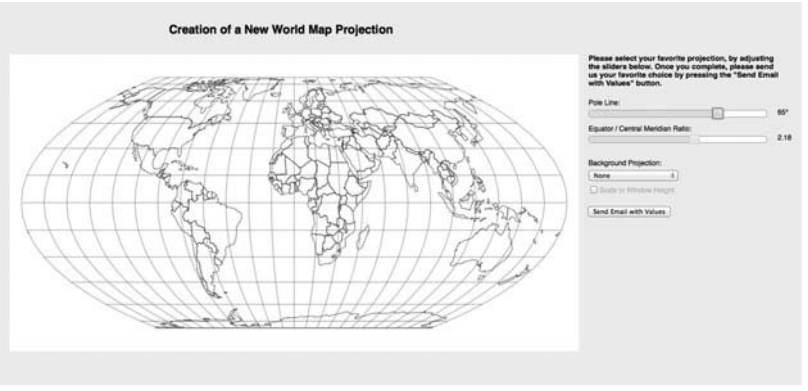

Figure 5. The web application designed for the user study. Sliders adjust the length of the pole line (the bounding parallel ϕ_B parameter of the transformation) and the equator/central meridian ratio p.

map projections during the last 10 years, or they are members of the International Cartographic Association (ICA) Commission on Map Projections.

The study participants opened a web application with a world map on the left and adjustable sliders on the right (Figure 5). The first slider adjusted the length of the pole line (the bounding parallel ϕ_B parameter of the transformation), and the second slider adjusted the equator/central meridian ratio p. For every change of the sliders, the map of the world interactively displayed a new pseudocylindrical projection, as shown in Figure 5. The dropdown menu below the sliders also enabled the display of three background projections for comparison: the Eckert IV, the Robinson, and the Natural Earth projection (Jenny *et al.* 2008, Šavrič *et al.* 2011). No distortion measures for the displayed projections were provided to the experts. Participants were asked to adjust the sliders and select their favorite choice based on their personal preference. When satisfied with their selection, they submitted the selected values via email. They were also invited to send comments concerning their suggested projection and the time they spent creating it.

5. Results and final selection

5.1. *Results of distortion analysis*

The computed indices D_{an} and D_{ab} (Equation 9) for all candidate projections can be represented in diagrams with the bounding parallel ϕ_B and the ratio p as variables. Figure 6 shows the mean angular deformation D_{an}, and Figure 7 shows the weighted mean error in the overall scale distortion D_{ab}. The horizontal axis represents the equator/central meridian ratio in both figures. The bounding parallel values vary along the vertical axis. The equator/pole line ratio q (Equation 7) is displayed on the right vertical axis of the diagram. Selected example graticules illustrate the candidate projections. Their locations on the diagram are marked with gray diamonds.

The projections with the lowest angular distortion D_{an} are those with a bounding parallel ϕ_B smaller than 50° and a ratio p between 2 and 2.7 (Figure 6). Projections with the lowest scale distortion D_{ab} are those with a bounding parallel ϕ_B between 35° and 75° and with a ratio p between 1.7 and 2.4 (Figure 7).

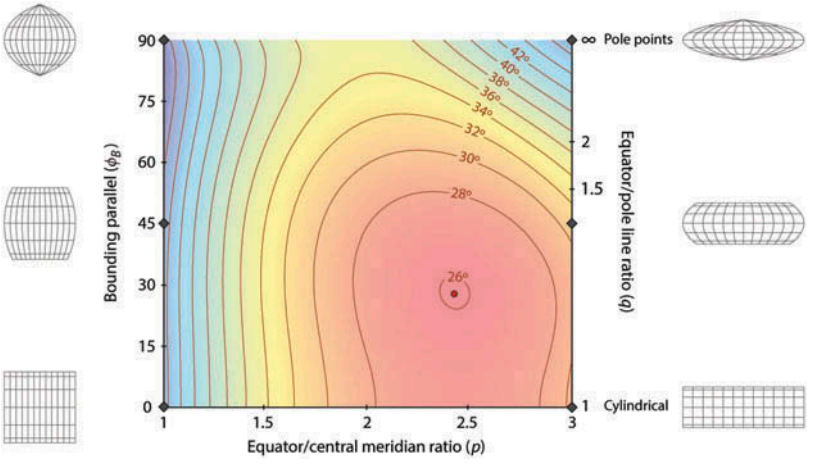

Figure 6. The mean angular deformation index for pseudocylindrical projections created by varying the bounding parallel ϕ_B and the equator/central meridian ratio p. Blue areas represent high mean angular distortion and red areas low mean angular distortion. The red dot on the diagram indicates the projection with the least mean angular distortion. Gray diamonds on the vertical axes mark locations of the sample graticules.

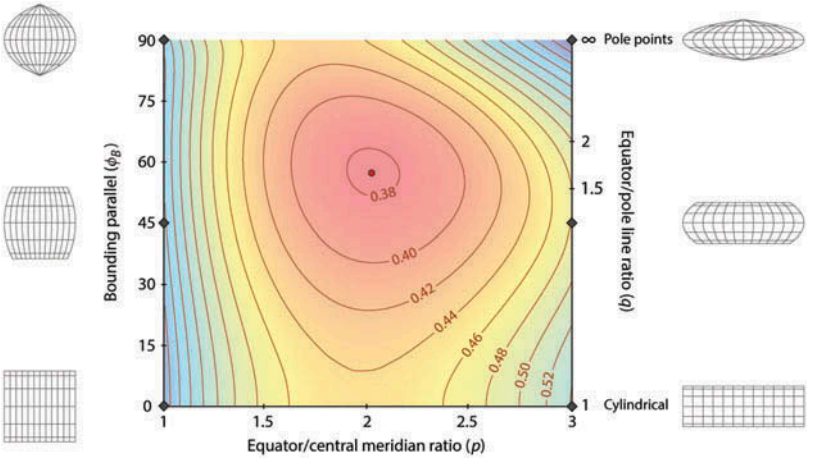

Figure 7. The weighted mean error in the overall scale distortion index for pseudocylindrical projections created by varying the bounding parallel ϕ_B and the equator/central meridian ratio p. Blue areas represent high mean scale distortion and red areas low mean scale distortion. The red dot on the diagram indicates the projection with the least mean scale distortion. Gray diamonds on the vertical axes mark locations of the sample graticules.

The red dots in Figures 6 and 7 indicate projections with the best distortion indices. The projection with the best mean angular deformation index is shown in Figure 8 (left). It has an equator/central meridian ratio of 2.43 and a bounding parallel at 28°. It has slightly bent meridians and the pole lines are almost the same length as the equator (the equator/pole line ratio q is 1.10). Its graticule resembles that of cylindrical equal-area projections, where areas close to the poles are strongly compressed in the north-south direction and stretched in the east-west direction.

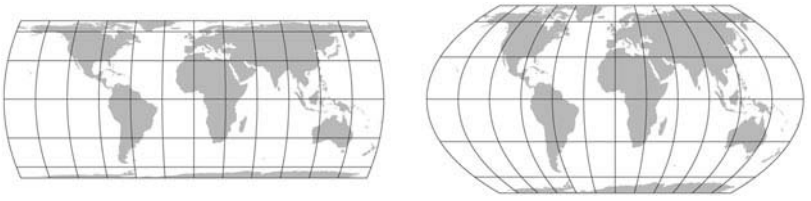

Figure 8. Pseudocylindrical projections with the lowest mean angular deformation index (left) and lowest weighted mean error in overall scale distortion index (right).

The projection with the best weighted-mean error in the overall scale distortion index is shown in Figure 8 (right). It resembles other well-known equal-area pseudocylindrical graticules, such as the Eckert VI, Wagner IV (Putninš P_2'), and Kavrayskiy VI (Wagner I). The projection has an equator/central meridian ratio of 2.02 and a bounding parallel at 57.5°. The equator is 1.63 times the length of the pole line. Compared to the projection with the best mean angular deformation index, the shapes of landmasses close to the poles are less distorted, and equatorial regions are slightly more stretched in the north-south direction because of a longer central meridian.

5.2. *Results of the user study*

Twenty-six experts participated in the study and submitted valid suggestions. In their comments, most experts stated that they tried to find a balance between the north-south stretching of the equatorial regions (caused by the equator/central meridian ratio) and the shape distortion of Australia, South America, and East or South-East Asia (caused by the convergence of the meridians). Most study participants reported not having used the background projections and having followed their personal aesthetic judgment, as they had been asked to do. Each of them spent 5–15 minutes for their selection.

Experts' suggestions included diverse graticules. All of them selected projections that show border meridians with a rounded shape and represent poles as lines. Figure 9 shows the experts' recommendations. The horizontal axis represents the equator/central meridian ratio p, and the bounding parallel ϕ_B values are along the vertical axis (as in Figures 6 and 7). Figure 9 displays selected graticules to illustrate the range of received suggestions. In the background of Figure 9, the weighted mean error in the overall scale distortion D_{ab} is shown by isolines.

Two patterns can be recognized in Figure 9. First, the equator/central meridian ratio is equal to 2 in many of the suggested projections. Exactly half of the experts stated in their comments that they first set the equator/central meridian ratio to 2, since this is equal to the real ratio. Then, they adjusted the length of the pole line to visually balance the distortion of the graticule.

The second pattern is that most of the suggested projections are similar to the projection with the best overall scale distortion, which is marked with a solid dot in Figure 9. Several experts even suggested projections that are very close to this projection, despite not having any information about the distortion properties and only relying on their personal visual judgment.

Taking into account the two patterns from Figure 9, two candidates for a pseudocylindrical projection can be extracted from the experts' suggestions. The first one is a projection computed from the arithmetic mean of the suggested values in which the

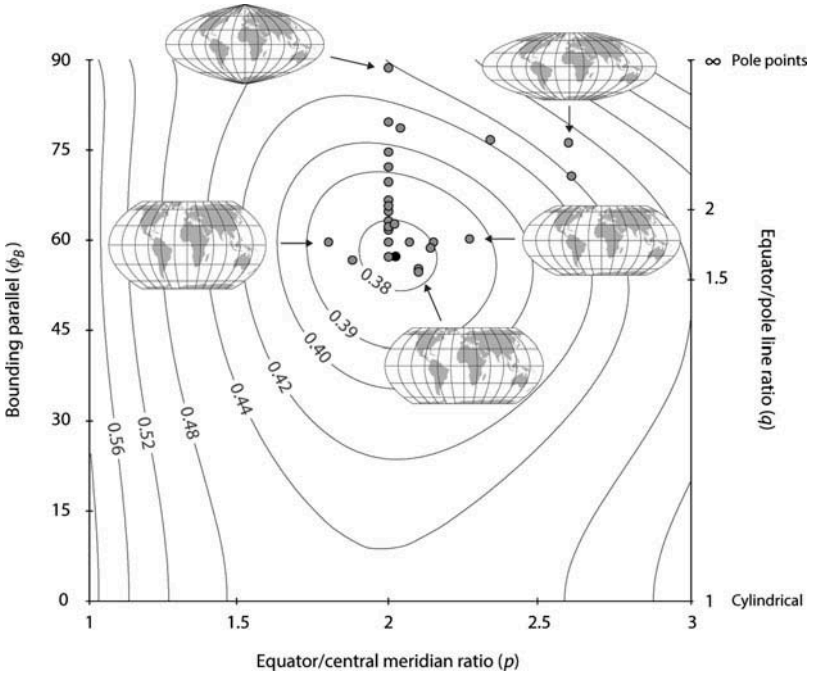

Figure 9. Projections suggested by 26 experts. Isolines indicate the weighted mean error in the overall scale distortion (as in Figure 7). A solid dot marks the projection with the best overall scale distortion.

weighted mean error in the overall scale distortion is less than 0.39 (18 projections). The result is a projection (Figure 10, left) with an equator/central meridian ratio of 2.03 and a bounding parallel at 61.9°. The projection is very similar to the projection with the best overall scale distortion, only the pole lines are slightly shorter (the equator is 1.82 times as long as the pole lines).

The second candidate can be extracted from projections with an equator/central meridian ratio of 2. The majority of these recommendations also have an equator/pole line ratio close to 2 (see Figure 9). Projections with such presumably aesthetically pleasing proportions were derived many times in the past, including the Eckert VI, Wagner IV, and Kavrayskiy VI. For these reasons, a projection with an equator/central meridian ratio p and an equator/pole line ratio q equal to 2 is selected as a second

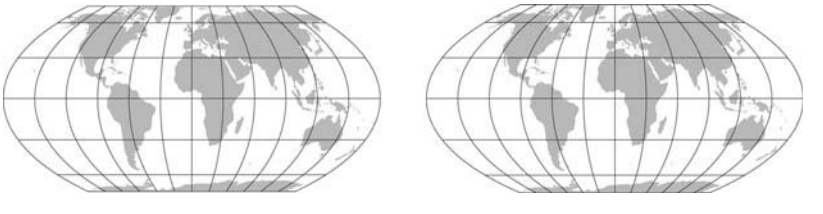

Figure 10. A pseudocylindrical projection from the arithmetic mean of the experts' suggestions (left) and a pseudocylindrical projection with an equator/central meridian ratio p and an equator/pole line ratio q equal to 2 (right).

candidate from the experts' suggestions. The projection has a bounding parallel at 65.1° (Figure 10, right).

5.3. *Final selection of a new equal-area pseudocylindrical projection*

The distortion analysis and the survey resulted in four pseudocylindrical candidate projections for inclusion in the adaptive composite map projections: (1) the projection with the best scale distortion index (Figure 8, right), (2) the projection with the best angular distortion index (Figure 8, left), (3) the projection from the mean values of suggested parameters, where the weighted mean error in the overall scale distortion is less than 0.39 (Figure 10, left), and (4) the projection with an equator/central meridian ratio and an equator/pole line ratio of 2 (Figure 10, right).

Tables 1 and 2 compare distortion indices of the four candidate projections and other projections that can be derived from the Lambert azimuthal projection using Wagner's transformation. Table 1 ranks projections based on the weighted mean error in the overall scale distortion index D_{ab} (Equation 9). The four candidate projections (except for the projection with the best angular distortion) have better weighted mean errors in the overall scale distortion index than the Hammer, the Eckert–Greifendorff, and the quartic authalic projections. All of the projections with pole lines (including the non-pseudocylindrical Wagner VII) have lower distortion indices than the projections showing poles as points.

Table 2 compares projections based on the mean angular deformation index D_{an} (Equation 9). As with scale distortion, the four candidate projections outperform the Hammer, the Eckert–Greifendorff, and the quartic authalic projections.

Table 1. Weighted mean error in the overall scale distortion.

Wagner VII	0.37
Best scale ($\phi_B = 57.5°$, $p = 2.02$)	**0.38**
Experts' mean ($\phi_B = 61.9°$, $p = 2.03$)	**0.38**
Ratios equal to 2 ($\phi_B = 65.1°$, $p = 2$)	**0.38**
Best angular ($\phi_B = 28°$, $p = 2.43$)	**0.43**
Hammer	0.43
Eckert–Greifendorff	0.45
Quartic authalic	0.47

Table 2. Mean angular deformation index.

Best angular ($\phi_B = 28°$, $p = 2.43$)	**25.96**
Best scale ($\phi_B = 57.5°$, $p = 2.02$)	**29.50**
Experts' mean ($\phi_B = 61.9°$, $p = 2.03$)	**30.27**
Wagner VII	30.71
Ratios equal to 2 ($\phi_B = 65.1°$, $p = 2$)	**31.00**
Eckert–Greifendorff	35.50
Hammer	35.66
Quartic authalic	36.00

The meridians of the projection with the best angular distortion are slightly curved, which results in a graticule that is similar to that of cylindrical projections (Figure 8, left). The projection considerably compresses polar areas in the north-south direction and stretches the same areas in the east-west direction. Furthermore, the projection has the largest weighted mean error of overall scale distortion among all of the candidates. For these reasons, it can be expected that cartographers would not routinely apply this projection for a world map.

The other three pseudocylindrical projections have similar appearances, and their weighted mean error for overall scale distortion values are identical (Table 1). They differ slightly based on the lengths of the central meridian and the pole line. The pseudocylindrical projection derived using the arithmetic mean has a better mean angular deformation index than the projection with ratios of 2. Hence, this pseudocylindrical projection is recommended for inclusion in the adaptive composite map projection technique (Figure 10, left).

6. Conclusion

Wagner's transformation method extends the set of equal-area small-scale map projections for adaptive composite map projections. In particular, pseudocylindrical projections can be created that represent poles as lines. We suggest a new equal-area pseudocylindrical projection based on distortion analysis and a user study of projection experts. The parameters for Wagner's transformation of this projection use a bounding parallel $\phi_B = 61.9°$ and an equator/central meridian ratio $p = 2.03$ (Equations 5 and 6, Figure 10, left). The suggested pseudocylindrical projection has better mean scale distortion than the Hammer, the Eckert–Greifendorff, or the quartic authalic projections suggested for the original adaptive composite map projections.

To transform the projection to the Lambert azimuthal projection, the parameters transition to $\lambda_B = 180°$, $\phi_B = 90°$, and $p = \sqrt{2}$ (Equations 3 and 4). This transition is accomplished with a linear interpolation when the user adjusts the map extent. The equal-area property is maintained throughout the transition, and inverse projection equations exist for the new projection and the transition.

In addition to the suggested pseudocylindrical projection, Wagner's transformation method enables the inclusion of two well-known map projections. The first projection is the cylindrical equal-area projection, which is not suitable for small-scale mapping because of its distortion characteristics, but it is useful at larger scales for mapping equatorial areas. The second projection is the Wagner VII (with $\lambda_B = 60°$, $\phi_B = 65°$, and $p = 2$). The Wagner VII projection has advantageous distortion properties (see Tables 1 and 2). The map author now has a choice between the Wagner VII projection with curved parallels and less distortion in peripheral areas and the new pseudocylindrical projection with straight parallels and moderately larger distortion in peripheral areas.

Acknowledgements

The authors thank Temenoujka Bandrova, Sarah E. Battersby, İ. Öztuğ Bildirici, Rolf Böhm, Mike Bostock, Frank Canters, Keith C. Clarke, Juliane Cron, Michael Finn, W. Randolph Franklin, Mátyás Gede, Matthew Gregory, Fritz Kessler, A. Jon Kimerling, Karen A. Mulcahy, Tom Patterson, Paweł Pędzich, John J. G. Savard, René Sieber, Ernst Spiess, Daniel Strebe, Waldo Tobler, Dražen Tutić, E. Lynn Usery, Robert J. Werner, Denis White, and Jarke J. van Wijk for participating in the user study and submitting their suggestions and valuable comments. The support

of Esri is greatly acknowledged, including valuable discussions with David Burrows, Scott Morehouse, and Dawn Wright. The authors also thank the anonymous reviewers for their comments.

References

Aitoff, D., 1889. Projections des cartes géographiques. *In*: *Atlas de géographie moderne*. Paris: Hachette.

Böhm, R., 2006. Variationen von Weltkartennetzen der Wagner-Hammer-Aïtoff-Entwurfsfamilie. *Kartographische Nachrichten*, 1, 8–16.

Bugayevskiy, L.M. and Snyder, J.P., 1995. *Map projections: a reference manual*. London: Taylor & Francis.

Canters, F., 2002. *Small-scale map projection design*. London: Taylor & Francis.

Canters, F. and Decleir, H., 1989. *The world in perspective: a directory of world map projections*. Chichester: John Wiley and Sons.

Čapek, R., 2001. Which is the best projection for the world map? *In*: *Proceedings of the 20th International Cartographic Conference*, 6–10 August 2001, Vol. 5. Beijing, China: LOC of ICC, 3084–3093.

Craster, J.E.E., 1929. Some equal-area projections of the sphere. *The Geographical Journal*, 74, 471–474. doi:10.2307/1783643

Evenden, G.I., 2008. *libproj4: A comprehensive library of cartographic projection functions (preliminary draft)* [online]. Available from: http://home.comcast.net/~gevenden56/proj/manual.pdf [Accessed 10 December 2013].

Goldberg, D.M. and Gott, J.R., 2007. Flexion and skewness in map projections of the earth. *Cartographica: The International Journal for Geographic Information and Geovisualization*, 42 (4), 297–318. doi:10.3138/carto.42.4.297

Jenny, B., 2012. Adaptive composite map projections. *IEEE Transactions on Visualization and Computer Graphics (Proceedings Scientific Visualization/Information Visualization)*, 18 (12), 2575–2582. doi:10.1109/TVCG.2012.192

Jenny, B. and Patterson, T., 2013. Blending world map projections with Flex projector. *Cartography and Geographic Information Science*, 40 (4), 289–296. doi:10.1080/15230406.2013.795002

Jenny, B., Patterson, T., and Hurni, L., 2008. Flex projector – interactive software for designing world map projections. *Cartographic Perspectives*, 59, 12–27.

Jenny, B. and Šavrič, B., in Press. Combining world map projections. *In*: M. Lapaine and E.L. Usery, eds. *Choosing a map projection*. Berlin: Springer.

Maling, D.H., 1974. Personal projections. *Geographical Magazine*, 46, 599–600.

Šavrič, B., *et al.*, 2011. A polynomial equation for the natural earth projection. *Cartography and Geographic Information Science*, 38 (4), 363–372. doi:10.1559/15230406384363

Siemon, K., 1936. Die Ermittlung von Kartenentwürfen mit vorgegebener Flächenverzerrung. *Deutsche Mathematik*, 1, 464–474.

Siemon, K., 1937. Flächenproportionales Umgraden von Kartenentwürfen. *Mitteilungen des Reichsamts für Landesaufnahme*, 13 (2), 88–102.

Siemon, K., 1938. Flächenproportionales Umbeziffern der Punkte in Kartenentwürfen. *Mitteilungen des Reichsamts für Landesaufnahme*, 14, 34–41.

Smyth, C.P., 1870. *On an equal-surface projection and its anthropological applications*. Edinburgh: Edmonton & Douglas.

Snyder, J.P., 1987. *Map projections: a working manual*. Washington, DC: US Geological Survey.

Snyder, J.P., 1993. *Flattening the earth. Two thousand years of map projections*. University of Chicago Press.

Snyder, J.P. and Voxland, P.M., 1989. *An album of map projections.* U.S. Geological Survey professional paper 1453. Washington, DC: United States Government Printing Office.

Tobler, W.R., 1964. Some new equal area map projections. *Survey Review*, 17 (131), 240–243. doi:10.1179/sre.1964.17.131.240

Wagner, K.H., 1931. *Die unechten Zylinderprojektionen: Ihre Anwendung und ihre Bedeutung für die Praxis*. Doctoral dissertation. Mathematisch-Naturwissenschaftliche Fakultät, University of Hamburg.

Wagner, K.H., 1932. Die unechten Zylinderprojektionen. *Aus dem Archiv der Deutschen Seewarte*, 51, (4), 68.

Wagner, K.H., 1941. Neue ökumenische Netzentwürfe für die kartographische Praxis. *In*: E. Lehmann, ed. *Jahrbuch der Kartographie 1941*. Leipzig: Bibliographisches Institut. 176–202.

Wagner, K.H., 1949. *Kartographische Netzentwürfe*. Leipzig: Bibliographisches Institut.

Wagner, K.H., 1962. *Kartographische Netzentwürfe*. 2nd ed. Mannheim: Bibliographisches Institut.

Wagner, K.H., 1982. Bemerkungen zum Umbeziffern von Kartennetzen. *Kartographische Nachrichten*, 32, 211–218.